

Analysis of Non-Equilibrium Fluctuations In A Ternary Liquid Mixture

Henri Bataller¹ · Cédric Giraudet² · Fabrizio Croccolo^{1,3} · José Maria Ortiz de Zárate⁴

Received: 11 January 2016 / Accepted: 3 August 2016 / Published online: 16 August 2016
© Springer Science+Business Media Dordrecht 2016

Abstract From the benchmark values of the diffusion and thermodiffusion coefficients of the tetralin, isobutylbenzene and n-dodecane ternary mixture, and the published optical contrast factors, we have evaluated the theoretical amplitudes of the two composition modes of the refractive-index fluctuations. Shadowgraph experiments have been performed on ground, where the current theory is expected to be correct only for large wave vectors. Two decay times have been observed experimentally. The fastest one being related to the thermal diffusivity of the mixture, while the slower one to mass diffusion. Hence, it has not been possible to distinguish the two eigenvalues of the mass diffusion matrix, a problem also encountered in traditional light-scattering with ternary mixtures of similar-size molecules. Thus, to compare the measured Intermediate Scattering Function with theory, we fix the amplitudes and decay rates

to the benchmark values, use the wave number as a fitting parameter, and compare it to the experimental wave number. The good agreement between theory and experiments for the larger wave numbers validates the theory developed for the microgravity conditions.

Keywords Non-equilibrium · Fluctuations · Ternary · Mixture · Diffusion · Thermodiffusion

Introduction

It is known that not only gravitational segregation, but also thermodiffusion due to geothermal gradients, are two physical phenomena determining the vertical distribution of species in hydrocarbon reservoirs on Earth (Lira-Galeana et al. 1994; Høier and Whitson 2001; Ghorayeb et al. 2003; Montel et al. 2007). Thermodiffusion can also lead to convective unstable situations in particular cases (Galliero and Montel 2009). Even when all these influences are taken into account, the optimization of the production of a given reservoir is limited by the lack of experimental thermodiffusion data for multi-component mixtures in reservoir conditions. The Soret Coefficients in Crude Oil (SCCO) project aims at producing such data. In a first phase carried out in 2007, to avoid the gravity-induced convection, experiments were performed at a microgravity platform on board the satellite FOTON-M3. One binary, two ternaries and one quaternary mixtures were studied (VanVaerenbergh et al. 2009; Srinivasan and Saghir 2009; Touzet et al. 2011). The measurements were compared with molecular dynamics simulations and with theoretical calculations based on the Thermodynamics of Irreversible Processes. However, the conclusions were incomplete because of difficulties encountered during post flight

This article belongs to the Topical Collection: Advances in Gravity-related Phenomena in Biological, Chemical and Physical Systems

Guest Editors: Valentina Shevtsova, Ruth Hemmersbach

✉ Henri Bataller
henri.bataller@univ-pau.fr

¹ Laboratoire des Fluides Complexes et leurs Réservoirs, UMR-5150, Université de Pau et des Pays de l'Adour, 1 Allée du Parc Montaury, Anglet, France

² Erlagen Graduate School in Advanced Optical Technologies (SAOT), Friedrich Alexander Universität, Paul Gordan Straße 6, 91052 Erlagen, Germany

³ Centre National d'Etudes Spatiales (CNES), Paris, France

⁴ Departamento de Física Aplicada, Universidad Complutense, Plaza de las Ciencias 1, 28040 Madrid, Spain

analysis at the laboratories. Now, on the occasion of the China Sea well explorations, a second phase of the SCCO space experiment has been scheduled. The thermodiffusion behaviour of the binary mixture decane-pentane, the ternary mixture decane-heptane-pentane and the quaternary mixture decane-heptane-pentane-methane, at two pressures and at 50 °C, will be studied on-board the Shijian-10 (SJ-10) Chinese satellite during 2016 (Galliero et al. 2016). To assure the success of this new mission, both validating ground measurements and numerical simulations have been planned for the ternary mixture. In this paper we present the first results of one of such validating experiments based on the measurement of non-equilibrium (NE) fluctuations.

NE fluctuations in intensive variables in fluid systems display spatial long-range as well as diverging intensities for large wavelengths (Ortiz de Zárate and Sengers 2006). This divergence is prevented by gravity (Vailati and Giglio 1997) and/or confinement (Ortiz de Zárate and Sengers 2001). The experimental study of the dynamics of NE fluctuations by light-scattering methods provides interesting information about the fluid properties, including the molecular and Soret coefficients, as some of us demonstrated for binary mixtures (Croccolo et al. 2012, 2013). The technique has been adapted to high pressure, allowing the study of fluids of oil interest in reservoir conditions (Giraudet et al. 2014). For the analysis of the light scattered by NE fluctuations induced by the Soret effect in the systems of the SCCO/SJ10 mission, both experimental and theoretical developments for ternary systems are necessary. As a first step in this direction, recently, Fluctuating Hydrodynamics was applied to determine the spectra of NE concentration fluctuations induced by the Soret effect in a ternary mixture in microgravity (Ortiz de Zárate et al. 2014). Now, as a second step and proof of feasibility, we present in this paper dynamic shadowgraph experiments with the benchmark ternary mixture of tetralin, isobutylbenzene and n-dodecane at the composition 0.8-0.1-0.1 in mass fraction, at 25°C and atmospheric pressure (Bou-Ali et al. 2015). A comparison with the theory (Ortiz de Zárate et al. 2014) is performed for wave numbers in which gravity and confinement effects on NE fluctuations are expected to be negligible.

The remainder of the paper is organized as follows: “Theory and Methods” reports theory and methods relevant to the analysis, in “Results and Discussion” we provide results and discussion, and in “Conclusions” conclusions are drawn.

Theory and Methods

Thermodiffusion In a ternary mixture, there are two independent concentrations c_1 and c_2 that we take as mass fractions. Hence, there are two independent diffusion fluxes

\vec{J}_1 and \vec{J}_2 , and Fick’s law in isotropic systems is expressed by a 2×2 diffusion matrix $\underline{\underline{D}}$. Similarly, there exist two thermodiffusion coefficients, D'_{T1} and D'_{T2} , so that in the simultaneous presence of temperature and concentration gradients, mass diffusion fluxes in the center-of-mass frame of reference are expressed as Taylor and Krishna (1993)

$$\begin{aligned}\vec{J}_1 &= -\rho \left(D_{11} \vec{\nabla} c_1 + D_{12} \vec{\nabla} c_2 + D'_{T1} \vec{\nabla} T \right), \\ \vec{J}_2 &= -\rho \left(D_{21} \vec{\nabla} c_1 + D_{22} \vec{\nabla} c_2 + D'_{T2} \vec{\nabla} T \right),\end{aligned}\quad (1)$$

with D_{ij} the components of the diffusion matrix

$$\underline{\underline{D}} = \begin{bmatrix} D_{11} & D_{12} \\ D_{21} & D_{22} \end{bmatrix}, \quad (2)$$

where SI units of m^2s^{-1} are used, and ρ is the mass density of the mixture. In this paper the ternary mixture will be subjected to a uniform stationary temperature gradient $\vec{\nabla} T$, of magnitude ∇T , in the direction of the z-axis. Naturally the system evolves to a stationary state characterized by vanishing diffusion fluxes. Hence, Soret effect induces the appearance of steady concentration gradients that for isotropic mixtures are parallel (or antiparallel) to the temperature gradient, and whose magnitudes can be obtained from Eq. 1 as

$$\begin{bmatrix} \nabla c_1 \\ \nabla c_2 \end{bmatrix} = -\underline{\underline{D}}^{-1} \begin{bmatrix} D'_{T1} \\ D'_{T2} \end{bmatrix} \nabla T. \quad (3)$$

Thermodynamic Fluctuations Thermodynamic and hydrodynamic variables can be described by a macroscopic average value plus a mesoscopic fluctuating term (Landau and Lifshitz 1959). For systems in equilibrium the average variables are global (do not depend on space or time), while the fluctuations are local. A great deal of attention has been focused on that simpler equilibrium case for many decades. Nowadays equilibrium fluctuations are understood as a sort of white noise, i.e. fluctuations of all wavelengths have similar intensity, and they are responsible of phenomena like scattering of light by a homogeneous fluid. Equilibrium fluctuations are spatially short-ranged, except in the close vicinity of critical points.

An understanding of the physics behind NE fluctuations has only gradually developed in the last couple of decades (Dorfman et al. 1994). In the presence of a macroscopic gradient, the thermodynamic variables exhibit fluctuations that are drastically different from equilibrium ones. First, the intensity of NE fluctuations is strongly enhanced as compared to equilibrium. This enhancement can be as large as several orders of magnitude, depending on the accessible wave numbers. Moreover, NE fluctuations are always long-ranged, whatever the distance from critical conditions. NE fluctuations are strictly related to the transport properties of the fluid. That is why from NE fluctuations analysis one can determine simultaneously all transport coefficients,

like viscosity, thermal and solutal diffusion and thermodynamic coefficients.

In our recent theoretical paper (Ortiz de Zárate et al. 2014), Fluctuating Hydrodynamics was applied to determine the spectra of NE composition fluctuations induced by the Soret effect in a ternary mixture in microgravity conditions, and neglecting the effect of confinement. Next, we succinctly summarize those theoretical results that are relevant to our current purpose. Composition fluctuations around the steady state given by Eq. 3 are described by a time correlation matrix that can be expressed as Ortiz de Zárate et al. (2014):

$$\langle \delta c_i(\vec{q}, t) \delta c_j^*(\vec{q}, t + \Delta t) \rangle = C_{ij}^E(\vec{q}, \Delta t) + C_{ij}^{NE}(\vec{q}, \Delta t), \quad (4)$$

where $\delta c_i(\vec{q}, t)$ are the fluctuations in the concentration of the two independent components at a given time t and wave vector \vec{q} . In the right-hand side (RHS) of Eq. 4 one observes that such correlation matrix can be additively split into two components, one equilibrium $C_{ij}^E(\vec{q}, \Delta t)$ and one non-equilibrium $C_{ij}^{NE}(\vec{q}, \Delta t)$. Note that, due to the time-translational invariance of the steady state of Eq. 3, the correlation function depends only on the time difference Δt at which composition fluctuations are evaluated.

The equilibrium part of Eq. 4 is not observable in our setup. For the non-equilibrium part we (Ortiz de Zárate et al. 2014) obtained the time correlation matrix as the sum of two diffusive modes, namely:

$$\underline{C}^{NE}(\vec{q}, \Delta t) = \frac{\rho k_B T}{\nu} \frac{q_{\parallel}^2}{q^6} \left[\underline{A}_1^{NE} e^{-\hat{D}_1 q^2 \Delta t} + \underline{A}_2^{NE} e^{-\hat{D}_2 q^2 \Delta t} \right], \quad (5)$$

where ν is the kinematic viscosity of the mixture, k_B the Boltzmann constant and $q_{\parallel}^2 = q_x^2 + q_y^2$ the component of the fluctuation wave vector \vec{q} in the plane parallel to the walls. The eigenvalues of the diffusion matrix, \hat{D}_1 and \hat{D}_2 (see Eqs. 9 and 10 below) appear in the exponential decays, while the amplitude matrix of the first mode is expressed as:

$$\underline{A}_1^{NE} = \frac{\hat{D}_1 \underline{X} \underline{X}^T - \hat{D}_2 \left| \underline{D} \right| \underline{D}^{-1} \underline{X} \underline{X}^T \left(\underline{D}^{-1} \right)^T}{2 \left(\hat{D}_1^2 - \hat{D}_2^2 \right)}, \quad (6)$$

where, to make notation more compact, we introduced a “gradient” matrix

$$\underline{X} = \begin{bmatrix} \nabla_{c_1} & \nabla_{c_1} \\ \nabla_{c_2} & \nabla_{c_2} \end{bmatrix}. \quad (7)$$

For the amplitude matrix of the second mode \underline{A}_2^{NE} , one exchanges $1 \leftrightarrow 2$ in Eq. 6 (Ortiz de Zárate et al. 2014).

In the developments leading to Eq. 5 several approximations are adopted. One of the more relevant it is to take the

limit of large Lewis and Schmidt numbers, which uncouple composition from temperature and viscous fluctuations. As a consequence, NE temperature and viscous fluctuations are not covered by the theory currently available (Ortiz de Zárate et al. 2014). A complete theory for NE ternary mixtures that includes the coupling between composition, viscous and temperature fluctuations is still missing.

Refractive Index Autocorrelation Equation 5 gives the autocorrelation matrix of composition fluctuations. However, what is actually measured in single-wavelength optical experiments is the time correlation function of refractive index fluctuations. Hence, for the practical use of the theory, we deduce here from Eq. 5 the theoretical expression for the refractive index autocorrelation, namely:

$$\langle \delta n(\vec{q}, \Delta t) \delta n(\vec{q}, 0) \rangle = \left[\frac{\partial n}{\partial c_1} \quad \frac{\partial n}{\partial c_2} \right] \cdot \underline{C}^{NE}(\vec{q}, \Delta t) \cdot \begin{bmatrix} \frac{\partial n}{\partial c_1} \\ \frac{\partial n}{\partial c_2} \end{bmatrix}, \quad (8)$$

where $\frac{\partial n}{\partial c_i}$ are the optical concentration contrast factors for the experimental (single) wavelength. In Eq. 8 we implicitly assume that equilibrium fluctuations (as well as NE temperature or viscous fluctuations) are unobservable. When substituting Eq. 5 into Eq. 8, we obtain an expression only valid in microgravity conditions, and that does not account for boundary (confinement) effects. However, in ground conditions, the result of substituting Eq. 5 into Eq. 8 is still correct for the asymptotic regime of large wave number $q \gg L^{-1}$, where L is the size of the system in the direction of the gradient. In that regime gravity and/or confinement effects are negligible (Ortiz de Zárate and Sengers 2001, 2006).

As further elaborated below, for the validation of the theory we compared experimental and theoretical refractive index autocorrelations, using for the theoretical $\langle \delta n(\vec{q}, \Delta t) \delta n(\vec{q}, 0) \rangle$ benchmark values of the ternary mixture of tetralin, isobutylbenzene and n-dodecane with 0.8-0.1-0.1 mass fraction, at 25 °C and atmospheric pressure (Bou-Ali et al. 2015). From the benchmark diffusion matrix of Bou-Ali et al. (2015), we evaluate the eigenvalues as:

$$\hat{D}_1 = \frac{D_{22} + D_{11} - \sqrt{(D_{22} - D_{11})^2 + 4D_{12} \cdot D_{21}}}{2} = 5.48 \times 10^{-10} \text{ m}^2 \text{ s}^{-1}, \quad (9)$$

$$\hat{D}_2 = \frac{D_{22} + D_{11} + \sqrt{(D_{22} - D_{11})^2 + 4D_{12} \cdot D_{21}}}{2} = 7.25 \times 10^{-10} \text{ m}^2 \text{ s}^{-1}. \quad (10)$$

Note that the two eigenvalues are not very different, so that one can anticipate that the two relaxation modes will be difficult to separate in experiments.

Next, substituting Eq. 5 into Eq. 8 and after some algebraic manipulations, the resulting refractive index autocorrelation function can be expressed as:

$$\langle \delta n(\vec{q}, \Delta t) \delta n(\vec{q}, 0) \rangle = \frac{A}{q^4} \left[B e^{-\hat{D}_1 q^2 \Delta t} + (1 - B) e^{-\hat{D}_2 q^2 \Delta t} \right], \quad (11)$$

where two wave-number-independent parameters are introduced to represent an overall amplitude:

$$A = \frac{\rho k_B T}{\nu} \left[\frac{\partial n}{\partial c_1} \quad \frac{\partial n}{\partial c_2} \right] \cdot \left(\underline{A}_1^{NE} + \underline{A}_2^{NE} \right) \cdot \left[\frac{\partial n}{\partial c_1} \right], \quad (12)$$

and a relative amplitude of the two diffusive modes

$$B = \frac{\left[\frac{\partial n}{\partial c_1} \quad \frac{\partial n}{\partial c_2} \right] \cdot \underline{A}_1^{NE} \cdot \left[\frac{\partial n}{\partial c_1} \right]}{\left[\frac{\partial n}{\partial c_1} \quad \frac{\partial n}{\partial c_2} \right] \cdot \left(\underline{A}_1^{NE} + \underline{A}_2^{NE} \right) \cdot \left[\frac{\partial n}{\partial c_1} \right]} = 0.831. \quad (13)$$

Note that in Eq. 11 we adopted $\cong q_-$, since in shadowgraph experiments observable wave vectors are very small (Trainoff and Cannell 2002). The numerical value $B = 0.831$ in the RHS of Eq. 13 has been obtained without any adjustable parameter, directly from the benchmark values of the diffusion matrix and the thermodiffusion coefficients (Bou-Ali et al. 2015), optical contrast factors (Sechenyh et al. 2013), and the experimental conditions: $\nabla T = \Delta T/L$, with $L = 2$ mm and $\Delta T = 16$ °C, as further discussed in the description of the experimental set up below. Regarding the refractive index concentration derivatives, for our particular ternary mixture they have been measured by Sechenyh et al. (2013) at the same temperature and pressure at which our current experiments are performed. Particularizing for the wavelength 670 nm Eq. 1 of Sechenyh et al. (2013), we obtain the refractive-index derivatives for the composition of interest as:

$$\begin{bmatrix} \frac{\partial n}{\partial c_1} \\ \frac{\partial n}{\partial c_2} \end{bmatrix} = \begin{bmatrix} 0.143 \\ 0.089 \end{bmatrix}, \quad (14)$$

which are the numbers actually used to obtain $B = 0.831$ in Eq. 13.

Experimental Set-Up Our thermodiffusion cell (for a picture of the experimental set-up see Fig. 1 of Croccolo et al. 2012) consists of two square sapphire plates ($8 \times 40 \times 40$ mm³) kept at different temperatures by two Peltier elements (Kryotherm, TB-109-1.4-1.5 CH) with a central circular aperture ($\varphi = 13$ mm). The two square Peltier elements are driven by two temperature controllers making use of a proportional-integrating-derivative feedback system (Wavelength Electronics, TCS651) maintaining the temperature of the internal side of each Peltier device with a stability better than 1 mK RMS over 1 day. The excess heat at the other side of each Peltier is removed by circulating water from a thermostat bath inside two aluminum plates. The two sapphire windows are kept apart by four adjustable plastic spacers. In our experiments, we set the liquid layer thickness to $L = 2$ mm. The sample is horizontally confined within a Viton O-ring with an internal diameter $d = 25$ mm.

The cell is filled by means of two syringe needles piercing the Viton O-ring. During the filling procedure, the cell is inclined and the fluid is pushed through the bottom syringe, while air is removed through the top one. After filling, the two needles are carefully removed and the holes in the O-ring close due to the pressure exerted on it by the sapphire windows. Attention is paid to avoid air bubbles in the filling procedure.

Experiments have been performed with the ternary mixture of tetralin or 1,2,3,4-tetrahydronaphtalene (Sigma-Aldrich, 99 %), isobutylbenzene (Sigma-Aldrich, 99 %) and n-dodecane (Sigma-Aldrich, 99 %) at 0.8-0.1-0.1 mass fraction, mean temperature $T_{\text{mean}} = 25$ °C and atmospheric pressure. Components were used without further purification.

We perform our experiments by imposing a difference of temperature of $\Delta T = 16$ °C on the horizontally positioned thin cell, previously filled with the homogenous fluid mixture.

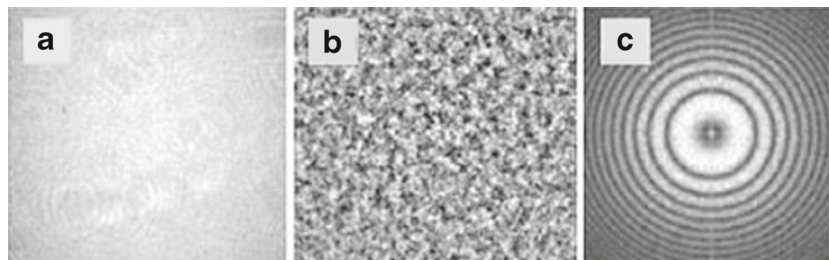


Fig. 1 Results of a near field scattering experiment (*shadowgraph layout*) on the ternary mixture of tetraline, isobutylbenzene and n-dodecane stressed by a thermal gradient ($\Delta T = 16$ °C). **a** 768×768 pix² near field image of the sample, $I(\vec{x}, t)$ **b** image

difference, $\Delta I(\vec{x}, \Delta t) = I(\vec{x}, t + \Delta t) - I(\vec{x}, t)$, having a correlation time of $\Delta t = 35$ ms and **c** 2D Fast Fourier Transform squared $|I(\vec{q}, t + \Delta t) - I(\vec{q}, t)|^2$ of **(b)**

In order to investigate NE fluctuations, it is common to use a scattering technique in the near field as the Shadowgraph (Wu et al. 1995), for which the physical optics treatment was given by Trainoff and Cannell (2002) and Croccolo and Brogioli (2011). The shadowgraph optical setup involves a low coherence light source (Super Lumen, SLD-MS-261-MP2-SM, $\lambda = 675 \pm 13$ nm) that illuminates the bottom of the cell through a single-mode fiber. The diverging beam exiting from the fiber end is collimated by an achromatic doublet lens ($L, f = 150$ mm, $\varphi = 50.8$ mm) and then passes through a linear film polarizer. In combination with a second linear polarizer after the cell it allows us to adapt the average transmitted light intensity. The detection plane is located at about $z = 95$ mm from the sample plane. As a sensor, we use a charge coupled device (AVT, PIKE-F421B) with 2048×2048 square pixels each of size $7.4 \times 7.4 \mu\text{m}^2$ and a dynamic range of 14-bit. Images were cropped within a $768 \times 768 \text{ pix}^2$ in order to reach the maximum acquisition frame rate of the camera.

Dynamic Near-Field Imaging Images acquired by means of a near-field scattering setup consist of an intensity map $I(\vec{x}, t)$ generated by the interference on the CCD plane between the portion of the incident beam that has passed undisturbed through the sample and the beams scattered by refractive index fluctuations occurring within the sample (Trainoff and Cannell 2002; Croccolo and Brogioli 2011). Statistical analysis involving fast Fourier transforms provides accurate measurements of the intensity $I_s(\vec{q}, t)$ of light scattered at each wave vector \vec{q} grabbed by the optical setup and for all the times t of the acquisition sequence. Different setups show different responses to the acquired signal as a function of the wave number q , which is described by the so-called transfer function $T(q)$.

Details of the quantitative dynamic analysis can be found elsewhere (Croccolo et al. 2006; Cerchiari et al. 2012). Here we just recall that the quantity directly obtained from the experiments is the so-called structure function $\langle |\Delta I_m(q, \Delta t)|^2 \rangle$, that is obtained by averaging (over all available times t in each image dataset and over the wave vector \vec{q} azimuthal angle) the individual spatial Fourier transforms of the shadowgraph image differences, like the one shown in the example of Fig. 1. This experimental structure function is theoretically related to refractive-index autocorrelation function by Croccolo et al. (2006), Croccolo et al. (2012), and Vailati et al. (2011):

$$\langle |\Delta I_m(q, \Delta t)|^2 \rangle = 2\{T(q)\langle \delta n(q, 0)^2 \rangle \times [1 - ISF(q, \Delta t)] + B(q)\}, \quad (15)$$

where the so-called intermediate scattering function is:

$$ISF(q, \Delta t) = \frac{\langle \delta n(q, \Delta t) \delta n(q, 0) \rangle}{\langle \delta n(q, 0)^2 \rangle}. \quad (16)$$

with $ISF(q, 0) = 1$. In Eq. 15, $T(q)$ is the optical transfer function and $B(q)$ the background noise of the measurement. It is implicitly assumed in Eq. 15 that the linear response of the CCD detector and any other electronic or electromagnetic proportionality parameters are aggregated inside $T(q)$ and/or $B(q)$. Sometimes the so-called structure factor $S(q)$, that is proportional to $\langle \delta n(q, 0)^2 \rangle$, appears in Eq. 15. It is worth noting that this approach does not require (at least for binaries) the knowledge of optical contrast factors (Croccolo et al. 2011a, b) conversely to other optical techniques.

Results and Discussion

Structure Function 10 different image acquisition runs have been performed with a delay time $dt_{\min} = 35$ ms of acquisition between two consecutive images, which corresponds to a mean frame rate of 28 Hz. Each set, containing 2000 images, has then been processed on a dedicated PC with a custom-made CUDA/C++ software, in order to perform a fast parallel processing of the images to obtain the structure functions $\langle |\Delta I_m(q, \Delta t)|^2 \rangle$, for all the wave numbers and for all the correlation times accessible within the image datasets. The temperature gradient is applied via two distinct temperature controllers, so that a linear temperature gradient sets up in some tens of seconds. The image acquisition is started about five hours later, to be sure that the concentration gradients due to the Soret effect are fully developed in the cell, a sufficiently large time compared to a vertical diffusion time across the layer thickness L of $\tau_d = L^2/D \approx 2\text{h}$ calculated with the smallest eigenvalue of the diffusion matrix.

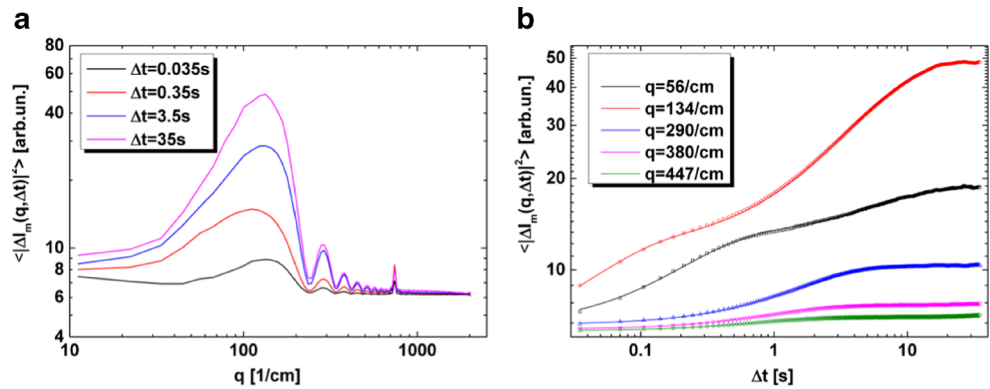
In Fig. 2 we present the mean structure function $\langle |\Delta I_m(q, \Delta t)|^2 \rangle$ of the 10 runs a) as a function of the wave number for different correlation times and b) as a function of the correlation time for different wave numbers. The oscillatory behavior shown in Fig. 2a is due to the optical transfer function $T(q)$ (see Eq. 15), it is typical of shadowgraph experiments and it corresponds to the ring pattern shown in Fig. 1c.

Figure 2a shows that for wave numbers $q > 400 \text{ cm}^{-1}$, the signal is completely lost in the background noise. Figure 2b shows that, for intermediate wave numbers, the time dependence of the structure function cannot be assumed to be mono-exponential. We therefore, decided to perform a quantitative analysis of the experimental structure functions by modeling the ISF as a double exponential, namely:

$$ISF(q, \Delta t) = a \exp\left(-\frac{\Delta t}{\tau_1(q)}\right) + (1 - a) \exp\left(-\frac{\Delta t}{\tau_2(q)}\right), \quad (17)$$

where τ_1 and τ_2 are two relaxation times. Hence, we performed fittings of the experimental $\langle |\Delta I_m(q, \Delta t)|^2 \rangle$ as a

Fig. 2 Experimental structure function $\langle |\Delta I_m(q, \Delta t)|^2 \rangle$ (a) as a function of the wave vector q for different correlation times Δt and (b) as a function of the correlation time Δt for different wave vectors q



function of Δt (see Fig. 2b) by substituting Eq. 17 into Eq. 15 and adopting as fitting parameters: the product $T(q) \langle \delta n(q, 0)^2 \rangle$, the background $B(q)$, the relative amplitude a , and the two decay times, τ_1 and τ_2 . For the fitting procedure we used a Levenberg-Marquardt Non-Linear Least Square fitting algorithm.

In Fig. 3 we show, as a function of the wave number, the two decay times obtained from the modeling of the ISF by Eq. 17. The horizontal dotted blue line corresponds to $dt_{\min} = 35$ ms, which is the physical limit of our experimental recording equipment. The two dotted lines represent the relaxation times $1/\hat{D}_1 q^2$ and $1/\hat{D}_2 q^2$ expected for the two concentration modes on the basis of the theory and the benchmark diffusion coefficients, see Eqs. 9 and 10.

The slowest decay time we were able to obtain from the experimental ISF, τ_2 in Fig. 3, is somehow in between the two theoretically expected concentration modes (at least for the range $q > 250 \text{ cm}^{-1}$ where the theory is valid).

Regarding the fastest experimental decay time, τ_1 in Fig. 3, we interpret it as coming from the decay of NE temperature fluctuations, not included in the current theory (Ortiz de Zárate et al. 2014). Unfortunately, it is not yet

available for a ternary mixture a complete NE fluctuations theory including temperature and the two concentration modes. However, from the corresponding theory for binary mixtures (Segrè and Sengers 1993) one expects that the decay time of NE temperature fluctuations (in the presence of gravity) will be given by Segrè and Sengers (1993):

$$\tau(q) = \frac{1}{\kappa q^2 \left[1 - \frac{Ra}{(qL)^4} \right]}, \tag{18}$$

where κ is the thermal diffusivity of the mixture and Ra the (thermal) Rayleigh number (note that when heating from above, the configuration adopted in our experiments, $Ra < 0$). As a guide to the eye we have added to Fig. 3, as a continuous red curve, Eq. 18 evaluated for our experimental conditions. An experimental value for the thermal diffusivity of the ternary mixture is unavailable, therefore, we adopted the thermal diffusivity of pure tetralin (the main component) instead: $\kappa = 8.6 \times 10^{-8} \text{ m}^2 \text{ s}^{-1}$. With all the due caution, the good agreement of Eq. 18 with the relaxation times of the experimental fast mode supports our claim that indeed τ_1 represents the relaxation time of the NE temperature fluctuations in the ternary mixture. The detection of this fast mode was possible because, as already mentioned, improvements in the shadowgraph set-up and its acquisition chain enabled us to achieve a minimum delay time between two successive images of 35 ms, therefore an approximate frame rate of 28Hz. In our previous studies the frame rate was about 8 Hz, which did not allow a good evaluation of the thermal fluctuations (the corresponding correlation function is fully decayed in the time interval between two successive images). The available theory (Ortiz de Zárate et al. 2014) was developed for the smaller frame rate and, consequently, temperature fluctuations were neglected. An extension of the theory to higher image acquisition frame rates is highly desirable, but outside of the scope of the current paper.

We conclude commenting Fig. 3 by pointing out that, on the one hand, for the smaller wave vectors confinement is expected to influence the dynamics of temperature NE fluctuations, although no theoretical or experimental

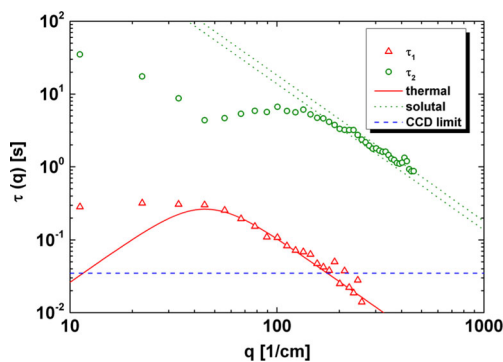


Fig. 3 Experimental decay times of NE fluctuations as obtained by fitting through Eqs. 15 and 17, as a function of the wave number q . Δ : fast mode, \circ : slow mode. The two green dotted lines represent the theoretical relaxation times, $1/\hat{D}_1 q^2$ and $1/\hat{D}_2 q^2$, of Eq. 5. The red solid curve represents Eq. 18 evaluated for the experimental gradient with the thermophysical properties of pure tetralin

investigation on this issue is available so far. In any case, the effect is expected to be different from the one on solutal NE fluctuations (Giraudet et al. 2015), since the boundary conditions are different. A definitive conclusion requires further extensions of the theory, something that is out of the scope of the current paper. On the other hand, for the larger wave vectors in Fig. 3, we conclude that it might be possible by our experimental technique to determine the thermal diffusivity of a ternary mixture.

Hence, as a summary, we conclude that we are able to evaluate two different decay times from the experimental $\langle |\Delta I_m(q, \Delta t)|^2 \rangle$ measured for a ternary mixture. The fastest decay time corresponds to the temperature fluctuations and the slowest decay time to a kind of average of the two theoretically expected concentration decay times. As already anticipated, the second conclusion is not unexpected because for a ternary mixture of similar-size molecules the two diffusive decay times are quantitatively very close, see Eqs. 9 and 10, and our implementation of dynamic light-scattering technique has not enough accuracy to distinguish between them. We note that a similar situation happens in traditional dynamic light-scattering (DLS) where, for a ternary mixture in equilibrium, the theory also predicts two concentration modes given by the two diffusion matrix eigenvalues that, so far, have not been clearly observed for mixtures of similar-size molecules (Bardow 2007), while a temperature mode and an ‘average’ concentration mode are routinely observed (Ivanov and Winkelmann 2008) similar to our findings here. Only very recently, by high-accuracy DLS experiments, two distinct mass diffusive modes have been unequivocally identified for gases dissolved in a binary mixture of hydrocarbons (Heller et al. 2015).

Before closing this section we should also comment about the deviations observed, for wavenumbers below $q < 250 \text{ cm}^{-1}$, between the slowest decay time τ_2 and the two diffusive relaxation times $1/\hat{D}_1 q^2$ and $1/\hat{D}_2 q^2$. We believe this is not an experimental artifact, but it is a real physical feature arising from gravity and/or confinement effects that are not accounted for by the theory for ternary mixtures available so far. If, as before, we use the case of binary mixtures as a guideline, we observe a striking resemblance between the behavior of the single average composition decay time $\tau_2(q)$ at small wavenumbers with what has been recently obtained for binary mixtures, and theoretically well-understood as indeed coming from the combined effect of gravity and confinement (Giraudet et al. 2015). We should stress that these deviations are not expected in microgravity conditions.

Theory Validation As summarized in the previous section, there are several difficulties in validating the current theory with our experiments performed on ground. First, the theory does not account for NE temperature fluctuations

that indeed are observed in the experiments. Second, the theory predicts two NE concentration modes that are undistinguishable in the experiments. Third, the combined effect of gravity and confinement are not taken into account by the available theory.

Hence, for validation, we adopted the approach of removing the thermal mode from the ISF and compare the remaining (solutal) signal with the theory of “Theory and Methods”. One can remove the contribution of temperature fluctuations from the ISF by using the model given by Eq. 17 to extract from the measured structure functions $\langle |\Delta I_m(q, \Delta t)|^2 \rangle$ a (normalized) experimental composition fluctuations intermediate scattering function as:

$$ISF_C(q, \Delta t) = \frac{1}{(1-a)} \left\{ 1 - \frac{\langle |\Delta I_m(q, \Delta t)|^2 \rangle - 2B(q)}{2T(q) \langle \delta n(q, 0)^2 \rangle} - a \exp\left(\frac{-\Delta t}{\tau_1}\right) \right\}, \quad (19)$$

where, for each wave number q , the fitted values of the product $T(q) \langle \delta n(q, 0)^2 \rangle$, the background $B(q)$, the relative amplitude a , and the decay time τ_1 of temperature fluctuations are used. As an example we show in Fig. 4 two ‘experimental’ $ISF_C(q, \Delta t)$ obtained by Eq. 19 for two different wave vectors as indicated.

According to the theory of “Theory and Methods”, the compositional $ISF_C(q, \Delta t)$ must be equal to:

$$\begin{aligned} ISF_C(q, \Delta t) &= \frac{\langle \delta n(q, \Delta t) \delta n(q, 0) \rangle}{\langle \delta n(q, 0)^2 \rangle} \\ &= 0.831 \exp\left(-5.48 \times 10^{-10} q^2 \Delta t\right) \\ &\quad + 0.169 \exp\left(-7.25 \times 10^{-10} q^2 \Delta t\right), \quad (20) \end{aligned}$$

where, as discussed earlier, known published thermophysical property values from independent sources were used for the numerical evaluation in the second line of Eq. 20.

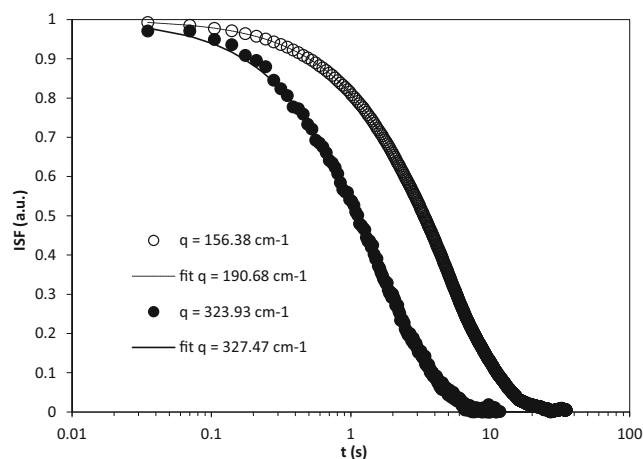


Fig. 4 Examples of fittings to the theory of experimental compositional ISF, measured at two different wave numbers q as indicated

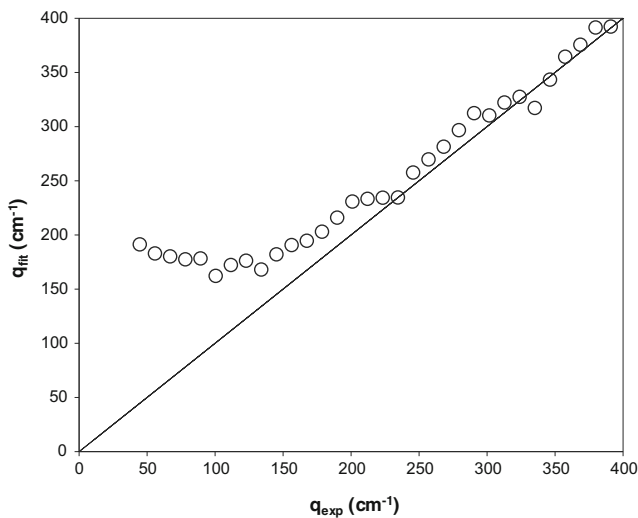


Fig. 5 Comparison between the wave numbers obtained from the theory q_{fit} and the experimental q_{exp} . The agreement is good for large $q \geq 250 \text{ cm}^{-1}$

Next, to systematically compare experiments with theory, we have fitted (as a function of Δt for all measured wave numbers) the experimental $ISFC(q_{\text{exp}}, \Delta t)$ obtained by Eq. 19 to the theoretical Eq. 20, using q in Eq. 20 as the only fitting parameter. As an example of these calculations, we added in Fig. 4 the curves resulting from the fitting for the two sets of experimental points. We observe that the theoretical curves represent quite well the experimental data, moreover, as shown in the legend inserted in the figure, for the larger wave number (for which the theory is expected to be valid) the wave number $q_{\text{fit}} \cong 327 \text{ cm}^{-1}$ obtained from the theory is undistinguishable from the actual wave number q_{exp} .

Finally, we report in Fig. 5 a comparison of the experimental q_{exp} with the theoretical q_{fit} in the whole available range of wave numbers. The solid line represents the 1:1 relation. We observe a very good agreement between experiments and theory, differences are $\sim 2\%$ at larger q and increase up to 5% at smaller q , as expected since the theory is for large q and, as discussed above, for wave numbers below $q < 250 \text{ cm}^{-1}$ gravity and confinement effects, not included in the current theory, are expected to play a significant role. In spite of the various limitations, both in the theory (not including temperature fluctuations) and in the experiments (inability of observing two concentration modes), we consider the agreement shown in Fig. 5 as quite satisfactory.

Conclusions

From benchmark values of the diffusion and thermodiffusion coefficients of the tetralin, isobutylbenzene and

n-dodecane ternary mixture, and the published optical contrast factors, we have evaluated for this particular mixture the amplitudes of the two composition modes of the refractive-index fluctuations as theoretically elucidated elsewhere (Ortiz de Zárate et al. 2014). Shadowgraph experiments have been performed on ground, where the current theory is expected to be correct only for large wave vectors. Two decay times have been observed experimentally. The first one is related to temperature fluctuations (neglected in the current theory for ternaries) that decay proportionally to the thermal diffusivity of the mixture, while the second decay time is related to mass diffusion. Thus, it has not been possible to distinguish experimentally the two eigenvalues of the mass diffusion matrix, a problem also encountered in traditional light-scattering with ternary mixtures of similar-size molecules. Hence, to compare the Intermediate Scattering Function associated to composition fluctuations with theory, we fix the amplitudes and decay rates to the benchmark values, use the wave vector as a fitting parameter, and plot the obtained q_{fit} vs. the real q_{exp} . The good agreement between theory and experiments for the larger wave vectors validates the theory developed for the microgravity conditions. The conclusions of this paper call for an extension of the fluctuating hydrodynamics of ternary liquid mixtures to include temperature fluctuations, as well as gravity and confinement effects. In that case, a better understanding of the shadowgraph experiments for all the experimentally accessible range of wave vectors is expected. On the other side, experiments with ternary mixtures with molecules which sizes are quite different will allow detection of the two distinct eigenvalues of the mass diffusion matrix; an example of this condition can be given by a solution of a polymer or a colloid in a binary solvent.

Acknowledgments This work has been supported by the European Space Agency through the SCCO project. JOZ acknowledges partial support from the Spanish State Secretary of Research under grant no. FIS2014-58950-C2-2-P. Support from the French space agency CNES is also acknowledged.

References

- Bardow, A.: On the interpretation of ternary diffusion measurements in low-molecular weight fluids by dynamic light scattering. *Fluid Phase Equilib.* **251**, 121–127 (2007)
- Bou-Ali, M.M., Ahadi, A., Alonso de Mezquia, D., Galand, Q., Gebhardt, M., Khlybov, O., Köhler, W., Larrañaga, M., Legros, J.C., Lyubimova, T., Mialdun, A., Ryzhkov, I., Saghir, M.Z., Shevtsova, V., Van Vaerenbergh, S.: Benchmark values for the Soret, thermodiffusion and molecular diffusion coefficients of the ternary mixture tetralin+isobutylbenzene+n-dodecane with 0.8-0.1-0.1 mass fraction. *Eur. Phys. J. E* **38**, 30 (2015)
- Cerchiari, G., Croccolo, F., Cardinaux, F., Scheffold, F.: Quasi-real-time analysis of dynamic near field scattering data using a graphics processing unit. *Rev. Sci. Instrum.* **83**, 106101 (2012)

- Croccolo, F., Brogioli, D., Vailati, A., Giglio, M., Cannell, D.S.: Use of the dynamic Schlieren to study fluctuations during free diffusion. *App. Opt.* **45**, 2166–2173 (2006)
- Croccolo, F., Brogioli, D.: Quantitative Fourier analysis of schlieren masks: the transition from shadowgraph to schlieren. *App. Opt.* **50**, 3419–3427 (2011)
- Croccolo, F., Arnaud, M.-A., Bégué, D., Bataller, H.: Concentration dependent refractive index of a binary mixture at high pressure. *J. Chem. Phys.* **135**, 034901 (2011a)
- Croccolo, F., Plantier, F., Galliero, G., Pijaudier-Cabot, G., Saghir, M.Z., Dubois, F., Van Vaerenbergh, S., Montel, F., Bataller, H.: Note: Temperature derivative of the refractive index of binary mixtures measured by using a new thermodiffusion cell. *Rev. Sci. Instrum.* **82**, 126105 (2011b)
- Croccolo, F., Bataller, H., Scheffold, F.: A light scattering study of non equilibrium fluctuations in liquid mixtures to measure the Soret and mass diffusion coefficient. *J. Chem. Phys.* **137**, 234202 (2012)
- Croccolo, F., Scheffold, F., Bataller, H.: Mass transport properties of the tetrahydronaphthalene/ndodecane mixture measured by investigating non equilibrium fluctuations. *C. R. Mec.* **341**, 378–385 (2013)
- Dorfman, J.R., Kirkpatrick, T.R., Sengers, J.V.: Generic Long-Range Correlations in Molecular Fluids. *Annu. Rev. Phys. Chem.* **45**, 213–239 (1994)
- Galliero, G., Montel, F.: Understanding compositional grading in petroleum reservoirs thanks to molecular simulations. Society of Petroleum Engineers Paper. 121902. Amsterdam (2009)
- Galliero, G., Bataller, H., Croccolo, F., Vermorel, R., Artola, P.-A., Rousseau, B., Vesovic, V., Bou-Ali, M., Ortiz de Zárate, J.M., Xu, S., Zhang, K., Montel, F.: Impact of Thermodiffusion on the initial distribution of Species in hydrocarbon reservoirs. *Microgravity Sci. Technol.* **28**, 79–86 (2016)
- Ghorayeb, K., Firoozabadi, A., Anraku, T.: Interpretation on the unusual fluid distribution in the Yufutsu gas-condensate field. *SPE J.* **8**, 114–123 (2003)
- Giraudet, C., Bataller, H., Croccolo, F.: High-pressure mass transport properties measured by dynamic near-field scattering of non-equilibrium fluctuations. *Eur. Phys. J. E* **37**, 107 (2014)
- Giraudet, C., Bataller, H., Sun, Y., Donev, A., Ortiz de Zárate, J.M., Croccolo, F.: Slowing-down of non-equilibrium fluctuations in confinement. *Europhys. Lett.* **111**, 60013 (2015)
- Heller, A., Chen, J., Fleys, M.S.H., van der Laan, G.P., Rausch, M.H., Fröba, A.P.: Investigation of Ternary Mixtures of n-Alkanes and Gases by Dynamic Light Scattering. 19th Symposium on Thermophysical Properties. Boulder (2015)
- Høier, L., Whitson, C.H.: Compositional grading-theory and Practice. *SPE Reserv. Evaluation Eng.* **4**, 525–532 (2001)
- Ivanov, D.A., Winkelmann, J.: Measurement of Diffusion in Ternary Liquid Mixtures by Light Scattering Technique and Comparison with Taylor Dispersion Data. *Int. J. Thermophys.* **29**, 1921 (2008)
- Landau, L.D., Lifshitz, E.M.: *Fluid Mechanics* Pergamon (1959)
- Lira-Galeana, C., Firoozabadi, A., Prausnitz, J.M.: Computation of compositional grading in hydrocarbon reservoirs. Application of continuous thermodynamics. *Fluid Phase Equilib.* **102**, 143–158 (1994)
- Montel, F., Bickert, J., Lagisquet, A., Galliero, G.: Initial state of petroleum reservoirs: A comprehensive approach. *J. Pet. Sci. Eng.* **58**, 391–402 (2007)
- Ortiz de Zárate, J.M., Sengers, J.V.: Fluctuations in fluids in thermal nonequilibrium states below the convective Rayleigh–Bénard instability. *Physica A* **300**, 25 (2001)
- Ortiz de Zárate, J.M., Sengers, J.V.: Hydrodynamic Fluctuations in Fluids and Fluid Mixtures. Elsevier, Amsterdam (2006)
- Ortiz de Zárate, J.M., Giraudet, C., Bataller, H., Croccolo, F.: Non-equilibrium fluctuations induced by the Soret effect in a ternary mixture. *Eur. Phys. J. E* **37**, 77 (2014)
- Sechenyh, V., Legros, J.C., Shevtsova, V.: Optical properties of binary and ternary liquid mixtures containing tetraline, isobutylbenzene and dodecane. *J. Chem. Thermodyn.* **62**, 64–68 (2013)
- Segrè, P.N., Sengers, J.V.: Nonequilibrium Fluctuations in Liquid Mixtures under the Influence of Gravity. *Physica A* **198**, 46–77 (1993)
- Srinivasan, S., Saghir, M.Z.: Measurements on thermodiffusion in ternary hydrocarbon mixtures at high pressure. *J. Chem. Phys.* **131**, 124508 (2009)
- Taylor, R., Krishna, R.: *Multicomponent Mass Transfer*. Wiley, New York (1993)
- Trainoff, S.P., Cannell, D.S.: Physical optics treatment of the shadowgraph. *Phys. Fluids* **14**, 1340–1363 (2002)
- Touzet, M., Galliero, G., Lazzeri, V., Saghir, M.Z., Montel, F., Legros, J.C.: Thermodiffusion: from microgravity experiments to the initial state of petroleum reservoirs. *Comptes Rendus - Mécanique* **339**, 318–323 (2011)
- Vailati, A., Giglio, M.: Giant fluctuations in diffusion processes. *Nature* **390**, 262 (1997)
- Vailati, A., Cerbino, R., Mazzoni, S., Takacs, C.J., Cannell, D.S., Giglio, M.: Fractal fronts of diffusion in microgravity. *Nat. Commun.* **2**, 290 (2011)
- VanVaerenbergh, S., Srinivasan, S., Saghir, M.Z.: Thermodiffusion in multicomponent hydrocarbon mixtures: Experimental investigations and computational analysis. *J. Chem. Phys.* **131**, 114505 (2009)
- Wu, M., Ahlers, G., Cannell, D.S.: Thermally induced fluctuations below the onset of the Rayleigh–Bénard convection. *Phys. Rev. Lett.* **75**, 17432–1746 (1995)